Chinese Journal of Chemical Engineering 69 (2024) 101–111

Contents lists available at ScienceDirect

Chinese Journal of Chemical Engineering

journal homepage: www.elsevier.com/locate/CJChE

Full Length Article

Phosphotungstic acid ionic liquid for efficient photocatalytic desulfurization: Synthesis, application and mechanism

Chenchao Hu [1], Suhang Xun [1, 3, *], Desheng Liu [1], Junjie Zhang [1], Minqiang He [2], Wei Jiang [2], Huaming Li [2], Wenshuai Zhu [2]

[1] *Institute of Environmental Health and Ecological Security, School of Environment and Safety Engineering, Jiangsu University, Zhenjiang 212013, China*
[2] *School of Chemistry and Chemical Engineering, Institute for Energy Research, Jiangsu University, Zhenjiang 212013, China*
[3] *Jiangsu Collaborative Innovation Center of Technology and Material of Water Treatment, Suzhou University of Science and Technology, Suzhou 215009, China*

ARTICLE INFO

Article history:
Received 25 November 2023
Received in revised form
7 February 2024
Accepted 18 February 2024
Available online 4 March 2024

Keywords:
Photocatalytic desulfurization
Extraction
Ionic liquid
CTAC-HPW

ABSTRACT

An efficient mass transfer process is a critical factor for regulating catalytic activity in a photocatalytic desulfurization system. Herein, a phosphotungstic acid (HPW) active center is successfully composited with a quaternary ammonium phosphotungstate-based hexadecyltrimethylammonium chloride ionic liquid (CTAC-HPW) by the ion exchange method for the photocatalytic oxidative desulfurization of dibenzothiophene sulfide. The keggin structure of HPW and highly mass transfer performance of organic cations synergistically enhanced the photocatalytic activity towards the effective convertion of dibenzothiophene (DBT) with the excitation of visible light. The deep desulfurization (<10 $mg \cdot kg^{-1}$) is attained within 30 min, and well stability is demonstrated within 25 cycles. Moreover, the CTAC-HPW photocatalyst projects well selectivity to interference from coexisting compounds such as olefins and aromatic hydrocarbons and universality of dibenzothiophenes, for example, 4-methyldibenzothiophene (4-MDBT) and 4,6-dimethyldibenzothiophene (4,6-DMDBT). Ultimately, a possible photocatalytic desulfurization mechanism is proposed according to the Gaschromatography-mass spectrometry (GC-MS), proving that the final product is the corresponding sulfone. The trapping experiment and electron spin resonance (ESR) analysis confirmed that h^+ and ·COOH played critical roles in the oxidation process. The work offers a practicable strategy for efficiently converting DBT to $DBTO_2$ with added value.

1. Introduction

The inevitable overuse of automotive fuel for the past several decades has given rise to the release of massive sulfur oxides (SO_x) into the atmosphere. These sulfur oxides are produced through the incomplete combustion of sulfur compounds found in diesel fuel [1,2]. It has been found that sulfur oxides play a critical role in air pollution, leading to the occurrence of acid rain, photochemical haze, construction corrosion, and adverse health effects [3,4]. The sulfur compounds, including thiols, disulfides, and thiophene sulfides, are the main contributors to the sulfur emissions in diesel fuel [5]. In response, many countries have implemented comprehensive measures to limit the concentration of sulfides in diesel fuels, and China has fully implemented the tougher standards, which are below 10 $mg \cdot kg^{-1}$ [6]. As the conventional desulfurization technique, hydrodesulfurization (HDS) has matured to be utilized to remove sulfur-containing harmful substances [7–10]. However, a severe reaction condition is necessary to remove the aromatic sulfur compounds, especially dibenzothiophene sulfides, through HDS, which causes massive energy consumption [11]. Therefore, developing alternative non-HDS technologies for deep desulfurization is extremely urgent. Several desulfurization processes have been developed to further the cleaning of oil, notably photocatalytic oxidative desulfurization (PODS), which has been studied due to the wide prospect of replacing HDS [12–17]. As a highly efficient and cost-effective alternative technology with mild reaction conditions and environmental friendly, PODS has garnered substantial attention from researchers [18]. Under the irradiation of

* Corresponding author. Tel.: +86 511 88790955.
E-mail address: xunsuhang@ujs.edu.cn (S. Xun).

https://doi.org/10.1016/j.cjche.2024.02.002

light, photogenerated electrons and holes are produced, as well as active radicals with strong oxidation properties such as superoxide radicals ($\cdot O_2^-$) and hydroxyl radicals ($\cdot OH$) [19,20]. The dibenzothiophene sulfide and its derivatives could be transformed into the corresponding sulfones or sulfoxides by radicals [21].

As a kind of efficient green solid acid, heteropoly acid (HPA) possesses a wide application prospect in photocatalysis, oxidation desulfurization, and organic synthesis. Composed of metal oxides and heteroatoms, HPA can be mainly divided into the categories of molybdenum-oxo clusters and tungsten-oxo clusters [22]. According to the structure of the molecular cluster, HPA is classified into Keggin type, Anderson type, Dawson type, Silverton type, and Waugh type [23–27]. Notably, most studies have focused on the unique Keggin-type $[XM_{12}O_{40}]^{n-}$ (X = Si or P, M = W or Mo), which contributed to its outstanding redox performance and multielectron transfer under ultraviolet and near-visible light irradiation [28]. However, as a homogeneous catalyst, the low specific surface area and poor solubility led to the agglomeration of active sites, poor mass transfer effect, and recycling ability, which limited the practical application of HPA [29]. These defects lead to its lower photocatalytic activity and the contamination of fuel with HPA. To improve the recoverable capacity and photocatalytic activity of photocatalysts, Craven *et al.* [30] loaded phosphotungstate on the alkylaminophosphazene functionalized silica and used it in oxidative desulfurization, proving that supported catalysts can effectively ameliorate the above problems. As a type of molten salt with outstanding solubility, stability, and structural variability, ionic liquids (ILs) have been successfully developed and recognized as a promising new type of solvent and precursor with outstanding physicochemical properties [31,32]. It is expected to realize the effective photocatalytic performance of the combination of organic cations and heteropolyanions that contributed to its well extraction and separation performance. In very recent years, Gao *et al.* [33] have designed a series of hybrid composites with varying carbon chain lengths based on [CnVP]Br with different carbon chain lengths, and they have high desulfurization efficiency under mild conditions. Significantly, the Keggin-type phosphotungstic acid ionic liquid displayed good desulfurization performance owing to the Brønsted acid active sites [34]. Wu *et al.* [35] prepared a $[TTPh]_3PW_{12}O_{40}$ which possesses the properties of ionic liquids and the keggin structure of heteropoly acids and demonstrated well desulfurization activity. Akopyan *et al.* [36] synthesized a series of polyoxometalate-based-IL catalysts and improved the desulfurization performance by regulating the Brønsted acidity. Furthermore, the imidazolium cation possesses the ability to extract and stabilize electrons as surface modifiers for photocatalysts, which leads to the separation of photogenerated e^--h^+ pairs with high efficiency [37]. These studies provide several ways of thinking for the research and development of high efficiency photocatalysts. Additionally, our investigation revealed a scarcity of reports on the photocatalytic desulfurization performance of heteropoly acid composite ionic liquids.

In this study, the quaternary ammonium phosphotungstate-based ionic liquid (CTAC-HPW) photocatalyst with keggin structure was prepared by combining the quaternary ammonium organic cation with the HPW anion, and the photocatalytic desulfurization performance of the prepared catalysts was studied. A process of extraction and photocatalytic oxidation desulfurization (EPODS) was pursued, using H_2O_2—HCOOH as oxidation and traditional ionic liquid [Hmim]Cl as extractant. The redox active sites possess exceptional photocatalytic properties, and deep desulfurization can be achieved within 25 cycling times. Furthermore, the reaction products and active radicals were studied, and a plausible mechanism was projected.

2. Materials and Methods

2.1. Materials

The necessary materials for the experiment and the synthesis method of the samples are reflected in the Supplementary Material.

2.2. Synthesis of the quaternary ammonium phosphotungstate-based ionic liquid material

Preparation process of hexadecyltrimethylammonium chloride (CTAC)/phosphotungstic acid (HPW) was shown in Fig. 1. 3 mmol of CTAC was dissolved in 50 ml distilled water as solution A and 1 mmol of HPW were dissolved in 20 ml distilled water as solution B. The yellow solution A dripped slowly into the solution B with 1 h stirring at room temperature. Afterward, the sediment was collected and washed with deionized water for 3 times and finally dried at 60 °C for 24 h.

2.3. Characterization

Fourier transform infrared spectroscopy spectra (FT-IR) were analyzed on Thermo scientific (Nicolet iS50). The thermal properties of the materials were measured by thermogravimetric (TG) analysis on STA-449C Jupiter (NETZSCH Corporation, Germany). The sample was tested from room temperature to 800 °C with a heating rate of 10 °C·min^{-1} under a nitrogen atmosphere. X-ray diffraction (XRD) patterns were used to determine the crystallinity obtained on a D8 ADVANCE X-ray diffractometer with a scanning speed of 7(°)·min^{-1} from 5° to 80°. X-ray photoelectron spectroscopy (XPS) data were acquired on the Thermo Scientific K-Alpha+. Elementary analyses

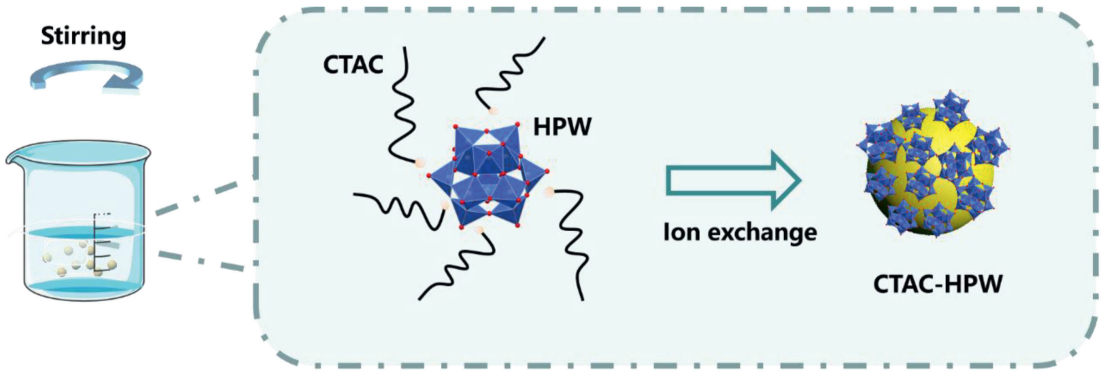

Fig. 1. The preparation process of CTAC-HPW.

were performed with CHN–O–Rapid (Heraeus Corporation). UV–vis diffuse reflectance spectra (DRS) were recorded on a UV–vis spectrophotometer (Shimadzu UV-2450, Japan) with $BaSO_4$ as the reference material. Gas chromatography (GC) (Agilent 7890A, HP-5 column, 30 m long × 0.32 mm inner diameter (id) × 0.25 μm film thickness) with a flame ionization detector (FID). The GC-MS analysis was carried out on an Agilent 7890A-5975C with an HP-5 (30 m) capillary column.

2.4. Extraction and photocatalytic oxidation desulfurization measurements

The desulfurization reaction was carried out on a photodegradation reactor GHX-3 with a 250 W xenon lamp. The model oil was prepared by dissolving 100 $mg \cdot kg^{-1}$ sulfur-containing substrates (dibenzothiophene (DBT), 4-MDBT, and 4,6-DMDBT) in *n*-octane. Then, 20 ml of model oil solution, 0.04 g of photocatalyst, and 1 ml of [Hmim]Cl were introduced into the reactor with water bath circulation. The mixture for two phases was first stirred magnetically and protected from light for 30 min to reach the establishment of extraction equilibrium. Next, 0.5 ml of H_2O_2 and 1 ml of formic acid were rapidly introduced with intense stirring. After that, the xenon lamp was turned on, and 1 μl of the upper oil phase samples were collected every 5 min. The sulfur content was analyzed using GC by employing tetradecane as an interior label standard. As for the recycling test, the model oil and catalyst, [Hmim]Cl, could be separated by centrifugation. The photocatalytic desulfurization performance was obtained using the following formula, where η stands for desulfurization rate, C_0 means initial sulfur concentration, and C_t represents the residual sulfur concentration after the reaction.

$$\eta = \frac{C_0 - C_t}{C_0} \times 100\% \quad (1)$$

3. Results and Discussion

3.1. Structure analysis of quaternary ammonium phosphotungstate-based ionic liquid material

The XRD analysis of pure HPW and CTAC-HPW is shown in Fig. 2 (a). The characteristic peak of HPW was surveyed in the range of 5°–10° (JCPDS 50-0656), which was attributed to the diffraction of the (110) crystal plane. A slight shift towards the lower angle can be discovered after the combination of CTAC, owing to the interaction between HPW and CTAC. The appearance of a wide peak located between 15° and 70° confirmed the transition to an amorphous state. The lack of diffraction peaks on additional crystal planes of HPW may be attributed to the presence of long carbon chains, which resulted in reduced crystallinity. In contrast to the crystal structure of pure HPW, the presence of electrostatic interaction and van der Waals force between cation and anion in the HPW-based ionic liquid enabled self-assembly [38]. To further investigate the structure of prepared photocatalysts, FT-IR analysis was conducted in Fig. 2. (b). The peak at 1080 cm^{-1} was ascribed to the P–O bond, and peaks at 983, 891, and 799 cm^{-1} were respectively attributed to the vibrational absorption of W-O_d, W-O_c-W, and W-O_d-W [39,40]. The results proved that the synthesized CTAC-HPW photocatalyst retained the Keggin structure of HPW. Furthermore, the peak at 2914 and 2850 cm^{-1} is due to the characteristic tensile vibration of quaternary ammonium compounds [41].

The elementary analysis was tested to explore the actual situation of ion exchange in the CTAC-HPW (Table S1). It was noteworthy that the calculated values were very close to the test values, indicating a successfully conducted ion exchange between CTAC and HPW with minimal loss. The C, N, and H were derived from the quaternary ammonium group of CTAC-HPW, and it basically conformed to the ratio of cationic and anionic molar ratio of 3:1. The results showed that the structures of anions and cations were preserved. The surface chemical states of the CTAC-HPW catalyst were additionally studied by means of the XPS technique. The survey spectrum exhibited that the elements W, O, C, N and P existed in the CTAC-HPW catalyst and no other impurity elements could be observed (Fig. 3 (a)). The banding energy peaks displayed at 36.4 and 38.6 eV were considered to be W 4f 7/2 and W 4f 5/2, demonstrating the presence of W^{6+} (Fig. 3 (b)) [42]. Furthermore, lower peaks at 35.2 and 37.5 eV can be observed, which belong to W^{5+}. The result may be due to the interaction of CTAC and HPW, and the electrons flow from CTAC to HPW after recombination. The variable-valence state provides more active sites for the photocatalyst. The O 1s spectra are shown in Fig. 3 (c). The banding energies of 531.2 and 532.6 eV were attributed to the W–O–W band and PO_4^{3-}, respectively [43,44]. Besides, bonds of C–C and C–N were extremely surveyed in high solution spectra, further confirming the preservation of the structure of the ionic liquid (Fig. 3 (d)) [45]. The result further confirmed the successful introduction of ionic liquid, and the structure of CTAC was reserved.

To further investigate the microstructure of the catalyst, scanning electron microscopy (SEM) was conducted on the CTAC-HPW. As shown in Fig. 4 (a), CTAC-HPW displayed a twisted stick shape,

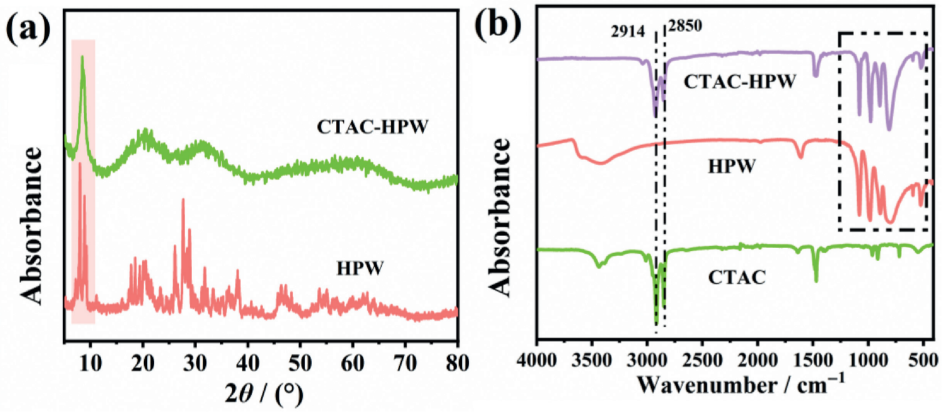

Fig. 2. XRD patterns of HPW and CTAC-HPW (a), FT-IR spectra of CTAC, HPW and CTAC-HPW (b).

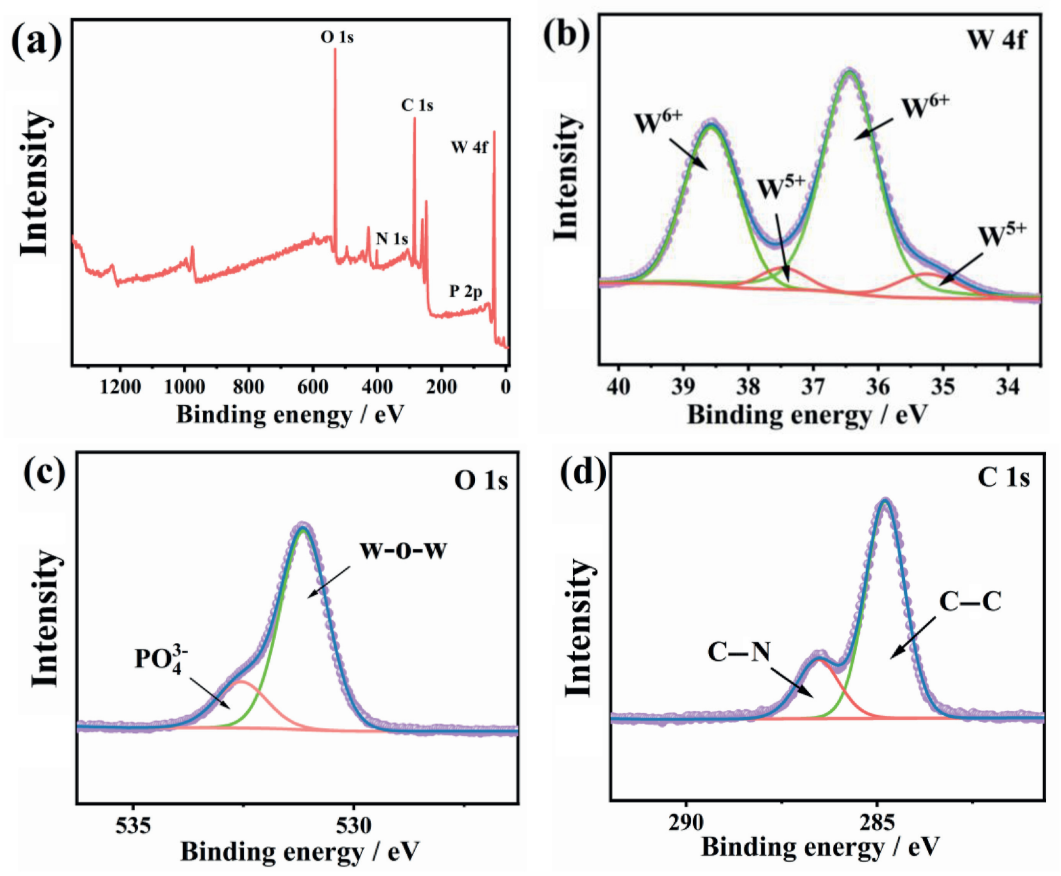

Fig. 3. The survey XPS spectrum (a) and high-resolution W 4f, O 1s and C 1s ((b)–(d)) of CTAC-HPW.

and small particles could be observed on the surface, which pertained to the phosphotungstic clusters. Energy-dispersive X-ray spectroscopy (EDS) elemental mapping was carried out to analyze the elemental composition and distribution on the surface of the catalyst [46,47]. The irregular morphology of ionic liquids conduced to the full exposure of active sites [48]. Elements C, N, P, W, and O were obviously surveyed and uniformly distributed on the surface of CTAC-HPW (Fig. 4 (b)–(h)). Moreover, the EDS spectrum further proved the existence of C, N, P, W, and O elements. The large amount of W distributed on the catalyst surface provided abundant active sites and greatly improved the desulfurization performance.

The UV–vis DRS spectrum revealed the light absorption properties of the CTAC-HPW [49]. As indicated in Fig. 5, the significant band-edge absorption of CTAC-HPW can be observed in the range of 210–270 nm and 316 nm, which could be interpreted as the absorption of electron transfer among the shared bridging O atoms and central W atoms on the WO_6 octahedron [50,51]. The peaks of W=O and W–O–W maintained the absorption characteristic of pure HPW (Fig. S1), and the obvious blue shift can be observed after the formation of CTAC-HPW. The phenomenon revealed the interaction between organic cations and heteropolyacid anions. It can be found that the absorption edge of the CTAC-HPW was about 405 nm in the range of visible light. The preliminary results showed that CTAC-HPW possessed positive absorption of visible light, conducing to increase the manufacture of photogenerated e^--h^+ pairs of CTAC-HPW and ultimately promoting photocatalytic desulfurization performance.

To investigate the thermal stability of the prepared photocatalyst, TG analysis was tested to investigate the structure and thermal stability (Fig. 6). The CTAC-HPW catalyst was one-step decomposition within 350–450 °C, indicating the decomposition of organic cationic and $[PW_{12}O_{40}]^{3-}$ anion. The conclusion suggested that the HPW-based ionic liquid organic-inorganic hybrids processed outstanding thermal stability and the structure can be fully preserved below 415.8 °C.

3.2. Desulfurization performance in extraction and photocatalytic oxidation desulfurization system

To investigate the role of different elements in an EPODS system, the impact of the introduction of visible light irradiation, CTAC-HPW, [Hmim]Cl, formic acid, and H_2O_2 on photocatalytic desulfurization efficiencies was discussed (Fig. 7 (a)). Under the reaction condition of only visible light irradiation, the EPODS performance was quite slow, at 10.9% in 30 min. With the addition of H_2O_2–HCOOH as the oxidant and visible light irradiation, the sulfur removal was 35.0% and 79.1%, respectively. However, when CTAC-HPW and [Hmim]Cl were introduced into the system simultaneously, the sulfur removal rose significantly to 99.1%, reaching the standard of deep desulfurization (S content <1 $mg \cdot kg^{-1}$). Based on the above results, the CTAC-HPW photocatalytic system demonstrated the excellent desulfurization performance. Under both the extraction of [Hmim]Cl and the oxidation of H_2O_2–HCOOH, the goal of deep desulfurization can arrive in the reaction process under visible light. The optimal reaction conditions for photocatalytic desulfurization were determined through a series of tests. Different ionic liquids were selected as extractants and investigated for their effects on desulfurization efficiency (Fig. 7 (b)). [Omim]PF_6, [Bmim]

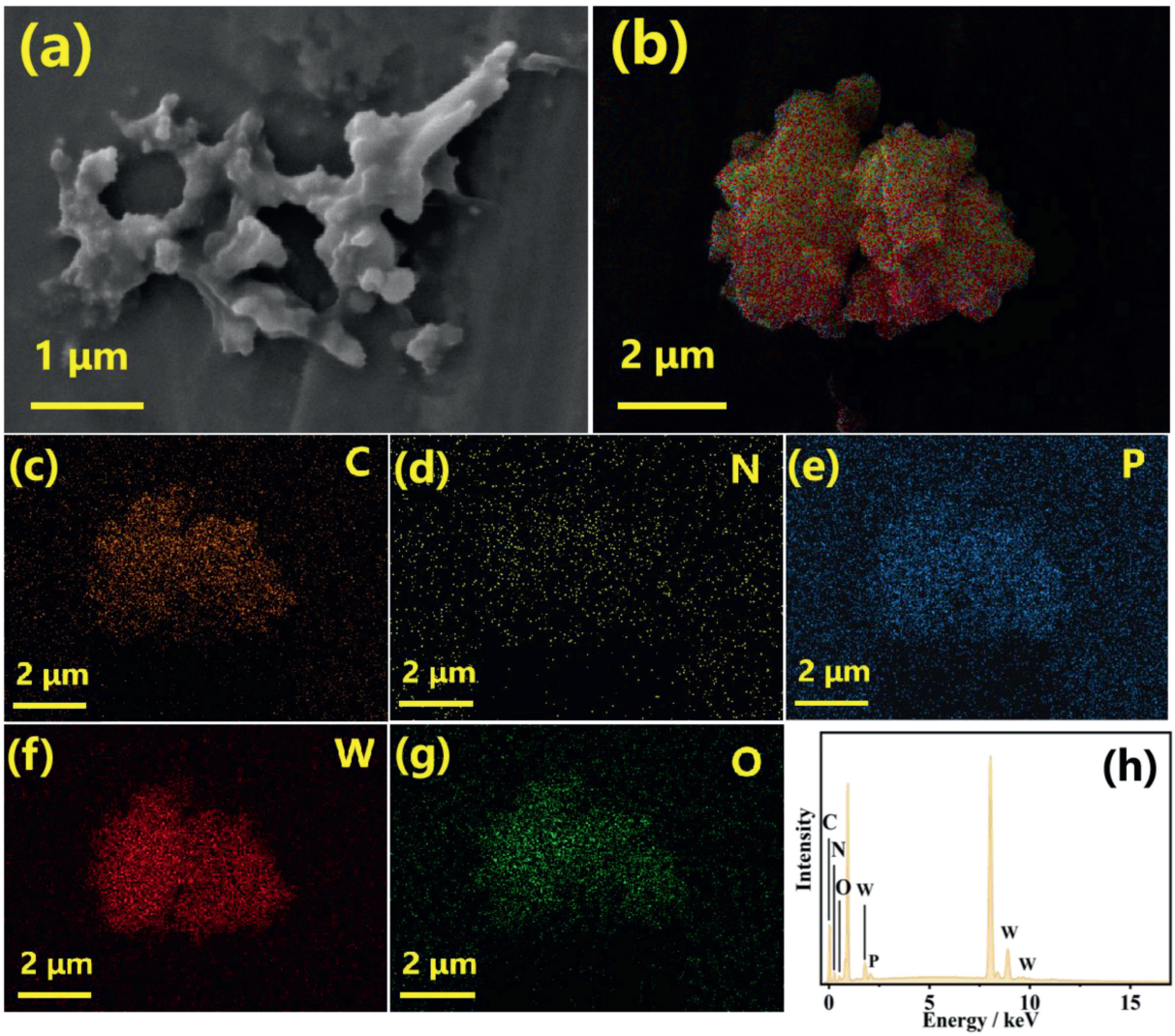

Fig. 4. (a) SEM images of CTAC-HPW; (b)–(g) Elemental mapping images of C, N, P, W, and O in CTAC-HPW. (h) EDS spectrum of CTAC-HPW.

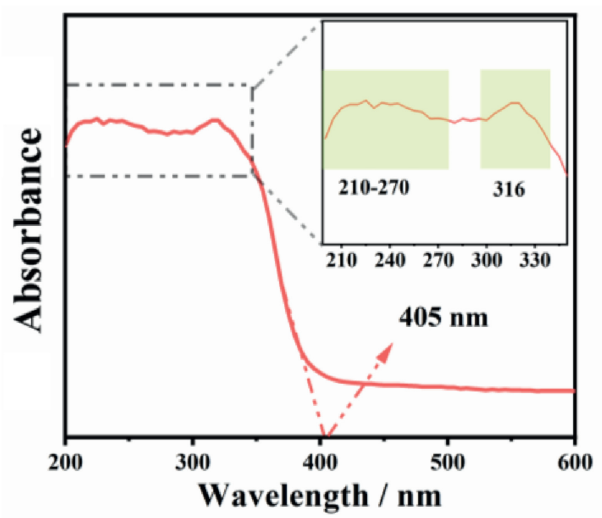

Fig. 5. UV–vis DRS spectrum of CTAC-HPW photocatalyst.

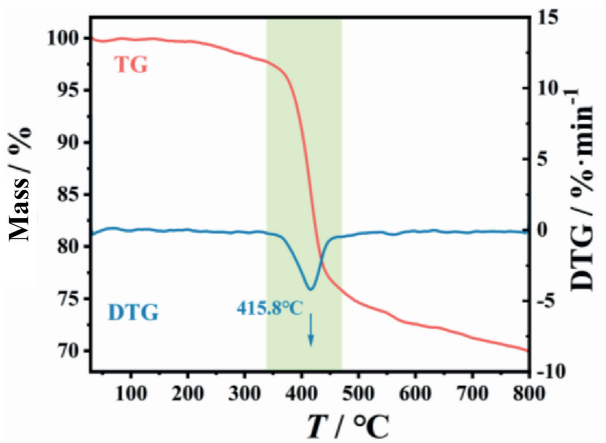

Fig. 6. Thermogravimetric and differential thermal curves of the CTAC-HPW catalyst.

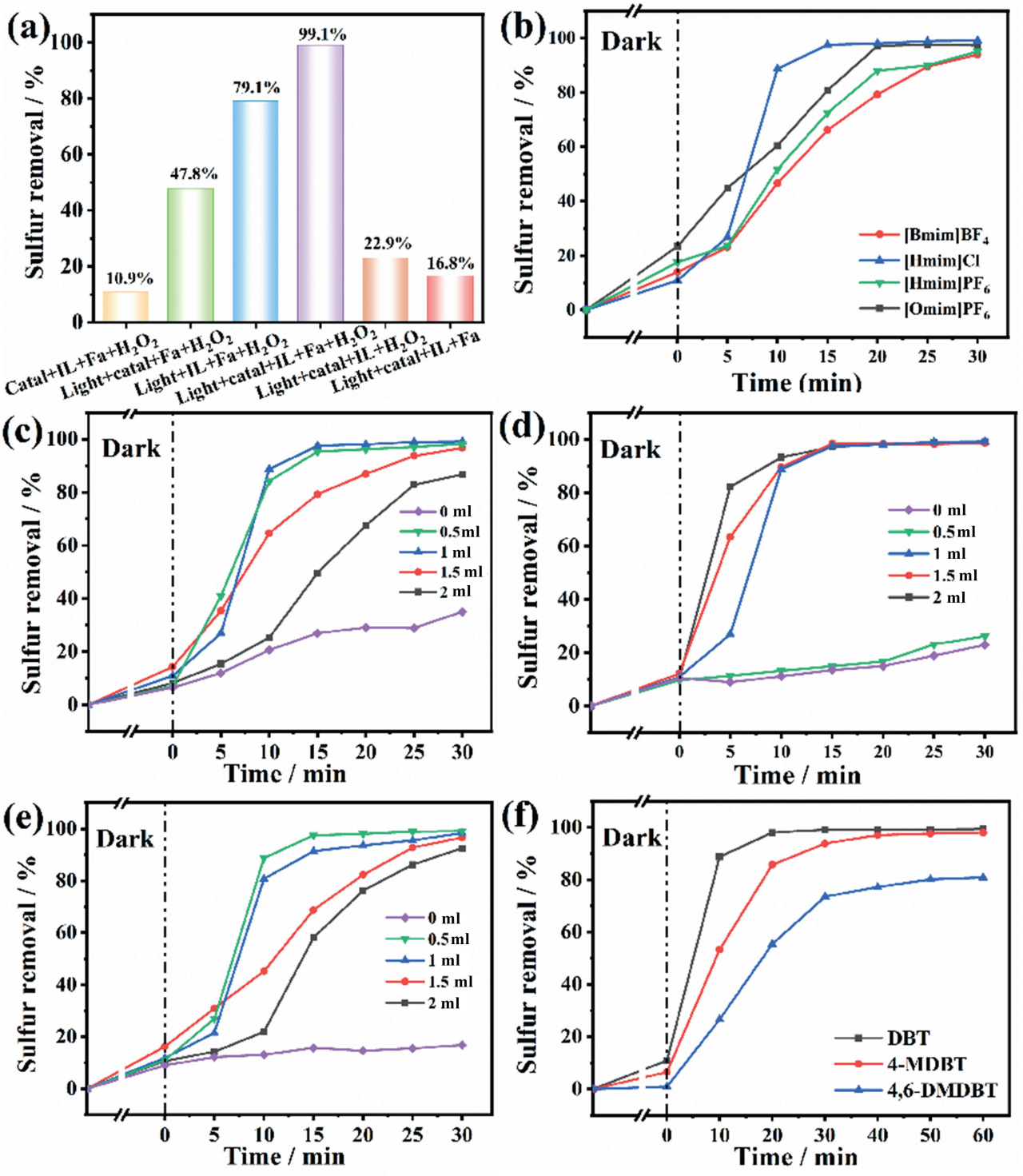

Fig. 7. Sulfur removal performance of different reaction systems (a). Effects of various EPODS conditions: The variety and dosage of the extractant variety (b–c), the used amount of HCOOH (d), and the addition amount of H_2O_2 (e). The photocatalytic activity of different sulfur-containing substrates (f). Conditions: T = 30 °C, V (model oil) = 20 ml, m (catal.) = 0.04 g, visible light, V ([Hmim]Cl) = 1 ml, V (HCOOH) = 1 ml, and V (H_2O_2) = 0.5 ml.

BF_4, [Hmim]PF_6, and [Hmim]Cl were selected as extractants, and the desulfurization efficiency ultimately complied with the following order: [Hmim]Cl > [Omim]PF_6 > [Hmim]PF_6 > [Bmim]BF_4. Therefore, [Hmim]Cl was chosen as the extractant in this system. Furthermore, the suitable dosage of extractant was discussed, and the amount of [Hmim]Cl showed a significant effect on DBT removal. While the dosage of [Hmim]Cl increased from 0 to 2 ml, the conversion efficiency of DBT gradually upgraded, and the optimum desulfurization activity could be obtained under the amount of [Hmim]Cl of 1 ml, indicating that the addition of [Hmim]Cl

ameliorated the mass transfer effect. The conversion of DBT was decreased to 86.7% as the volume of [Hmim]Cl increased to 2 ml, which may have resulted from the viscosity of ILs. Fig. 7 (c) revealed the effect of the dosage of HCOOH on the conversion of DBT. With the increase in volume of HCOOH from 0 ml to 2 ml, the desulfurization rate increased gradually, and the surfur content extremely fell to less than 1 $mg \cdot kg^{-1}$ within 30 min. When the content of HCOOH was 1 ml, the requirement of deep desulfurization could be achieved. Besides, in an effort to prevent the occurrence of excessive acid use and excessive acidity in model oil, 1 ml of HCOOH was finally selected as the most suitable dosage of prooxidant for the following desulfurization experiments. The influence of the H_2O_2 volume on the conversion of DBT is presented in Fig. 7 (d). A series of dosages of H_2O_2, including 0, 0.5, 1, 1.5, and 2 ml, were selected to investigate the effect of H_2O_2 on desulfurization performance in Fig. 7 (e). The increase in desulfurization efficiency may be attributed to the generation of more free radicals, but for more than 1 ml, with the excessive introduction of water, the mass transfer ability of the system was affected, and then the desulfurization capacity was decreased. The EPODS ability was upgraded from 16.8% to 99.1% as the H_2O_2 volume increased from 0 to 1 ml. As shown in the above results, the synergistic oxidative effect of H_2O_2 and formic acid facilitated the photocatalytic oxidation process. Furthermore, the desulfurization performance of CTAC-HPW was compared with different reported composite photocatalysts in Table 1, and an obvious advantage can be displayed [46,52–59].

To further study the catalytic activity of CTAC-HPW photocatalyst, DBT, 4-MDBT, and 4,6-DMDBT were analyzed (Fig. 7 (f)). It could be observed that the removal capacity followed the sequence: DBT > 4-MDBT > 4,6-DMDBT. The reactivity of diverse sulfur-containing substrates a significant discrepancy, and the ease of oxidation reactions is often positively correlated with the electron cloud density of the S atom [60]. Even though 4,6-DMDBT has a higher electron cloud density, the steric hindrance effect of two methyl groups may have had a greater influence on the oxidation reaction, leading to the slightly lower removal rate of 4,6-DMDBT [61].

3.3. Effect of oil composition for desulfurization of model oil

The influence of other organic compounds was also to be considered for the deep desulfurization of fuel oils in practical procedures. Consequently, cyclohexene and *p*-xylene were selected as interferers to explore the sulfur removal capacity of the photocatalyst in the presence of olefin and aromatic interferers, respectively. As shown in Fig. 8 (a), the sulfur removal was reduced from 99.4% to 40.0% and 98.4% in 60 min, respectively. Compared to the cyclohexene addition, the desulfurization rate did not decrease significantly in the presence of *p*-xylene. This may be due to the fact that olefin is easier to oxidize in a strong oxidizing environment, resulting in a competitive reaction between the DBT oxidation reaction and other compounds. In summary, the two comparative experimental results revealed that the aromatic hydrocarbons in the oil showed no notable impact for the desulfurization activity, and the cycloolefin had a significant effect on the desulfurization activity. Therefore, this system was more suitable for fuel oil containing a small amount of olefin.

3.4. The recyclability and stability of quaternary ammonium phosphotungstate-based ionic liquid material

The stabilization of the prepared photocatalysts was studied. After each activity experiment, the upper cleaning oil phase was poured out by the dumping method, leaving the [Hmim]Cl extractant and CTAC-HPW catalyst. Then 20 ml of new, uncleaned oil was introduced for one more desulfurization experiment. As shown in Fig. S2, the sulfur content can be controlled below 10 $mg \cdot kg^{-1}$ in each 30 min test during the first 24 cycles, demonstrating the outstanding stability of CTAC-HPW. Notably, the desulfurization performance showed a gradual decrease during the cycle test, which may have resulted from the coverage of active sites by the sulfone product. Thus, by extending the reaction time to 60 min, ultra-deep desulfurization can be achieved, and the spent catalyst remains high in desulfurization activity after 25 recycle times (Fig. 8. (b)). Moreover, as shown in Fig. 8. (c), the spent photocatalyst was basically identical with the original photocatalyst on the FT-IR spectra, and the Keggin structure of HPW was largely kept. The tensile vibration of C=O at 1722 cm^{-1} may originate from the residual formic acid in the reaction. The result implied that the catalyst possessed outstanding cycle performance and stability, which was tended to favor its applicable and continuous.

3.5. Extraction and photocatalytic oxidation desulfurization mechanism

To understand the active species of the CTAC-HPW during the conversion of DBT, control experiments were carried out with the radical scavengers. Here, Ethylenediaminetetraacetic acid disodium salt (EDTA-2Na), iso-Propyl alcohol (IPA), and 1,4-Benzoquinone (BQ) were selected to quench the active species of h^+, ·OH, and $\cdot O_2^-$, respectively. The conversion rate of DBT showed obvious

Table 1
Photocatalytic desulfurization performance of recently reported catalysts

Catalyst	Light source	*t*/min	Sulfur removal	Type of extractant	Recycle number	Ref.
CTAC-HPW	250 W Xe lamp, visible light	30	DBT: 99.1% 4-MDBT: 98% 4,6-DMDBT: 80.8%	[Hmim]Cl	25	This work
Mn–Co–Mo/Al_2O_3	/	5	DBT: 100%	/	6	[46]
$CuWO_4/SiO_2$	300 W Xe lamp, visible light	70	DBT: 93%	/	4	[52]
MoS_2–CeO_2/SiO_2–Al_2O_3	150 W Halogen, visible light	60	DBT: 93%	MeCN	5	[53]
MIP/AgP*x*	500 W visible light/UV	60	DBT: 98%	MeCN	6	[54]
$BiVO_4$–CuO-Clinoptilolite	400 W Osram lamp	30	DBT: 94.7%	MeCN	5	[55]
Ir/Pr-N-CQDs-TiO_2	UV	50	BT/DBT/4,6-DMDBT: 99.8%	/	11	[56]
NiO–Bi_2WO_6	Visible light	150	DBT:98.2% BT:95.37% TH:85.8%	MeCN	6	[57]
p-BiOI/*n*-$BiPO_4$	400 W Xe lamp, visible light	120	BT:95.0%	MeCN	5	[58]
$Ni_xZn_{2-x}V_2O_7/WO_4$	500 W visible light/UV	120	BT:95.0%	/	5	[59]

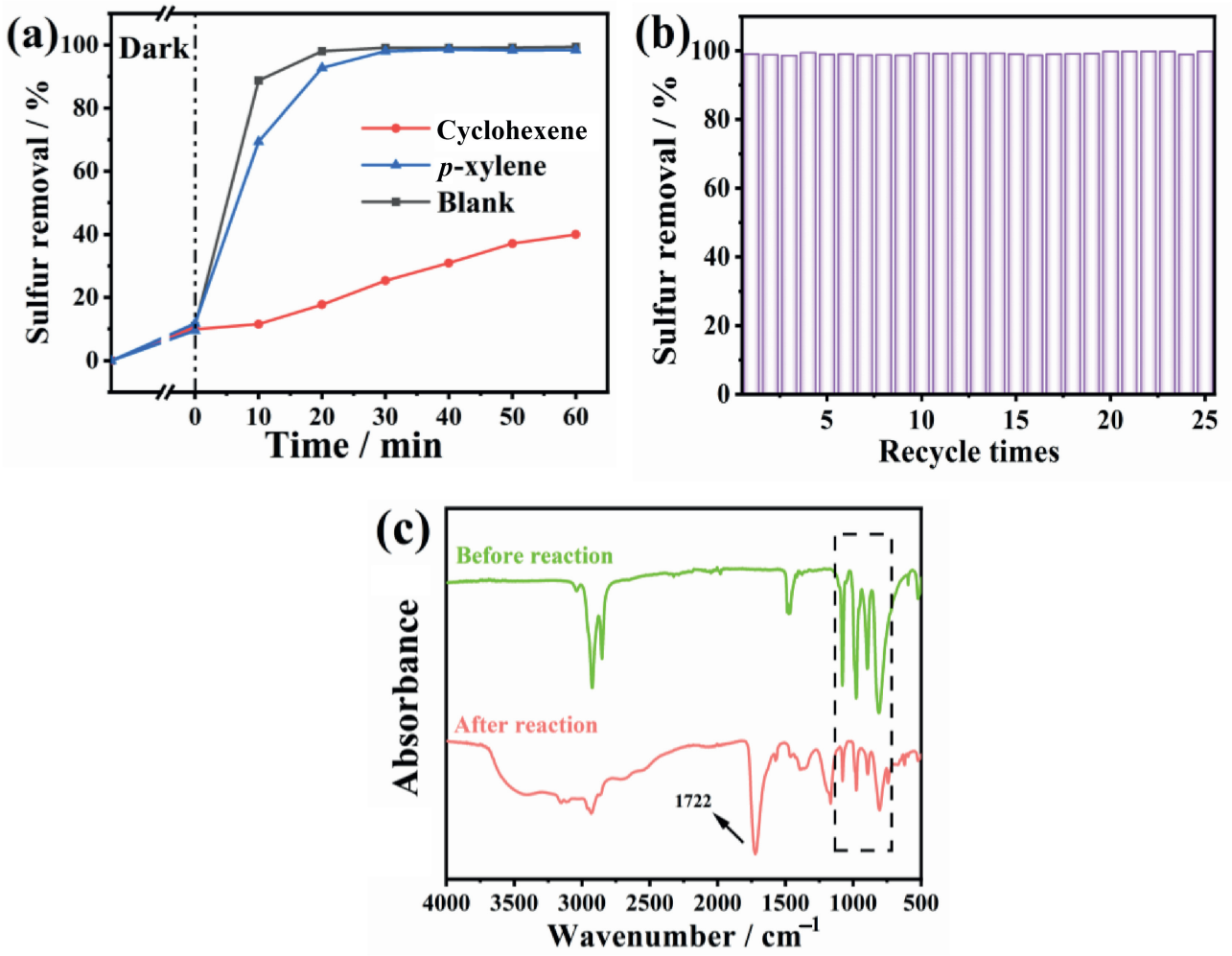

Fig. 8. (a) The impact of various interferences on the EPODS efficiency. (b) The recycle performance of CTAC-HPW within 60 min. (c) Comparison of FT-IR before and after the cycle. Conditions: $T = 30$ °C, V (model oil) = 20 ml, m (catal.) = 0.04 g, visible light, V ([Hmim]Cl) = 1 ml, V (HCOOH) = 1 ml, and V (H_2O_2) = 0.5 ml.

suppression after the introduction of EDTA-2Na, which decreased the rate from 99.1% to 29.5% (Fig. 9 (a)). In addition, the quenching of ·OH and $\cdot O_2^-$ displayed little influence on the desulfurization performance. The electron spin resonance (ESR) technology was carried out to further demonstrate the active radicals produced in this EPODS system. After adding Dimethyl pyridine N-oxide (DMPO) as a trapping agent, two kinds of ESR signals were detected. Notably, no apparent radical signals were observed in the absence of light. As seen from Fig. 9 (b), the quartet peaks with a characteristic intensity of 1:2:2:1 were assigned to the DMPO-·OH active species [62]. Furthermore, the six peaks were assigned to the RO· active species in Fig. 9. (c), which can be determined as ·COOH, and the possible formation process is shown in Eq. (2) [63,64]. The result indicated the synergies between H_2O_2 and HCOOH. Combined with the above experiments, h^+ and ·COOH played critical roles in the oxidation process, and there were other active species such as ·OH and $\cdot O_2^-$, which played a secondary role.

$$HCOOH + \cdot OH \rightarrow \cdot COOH + H_2O \quad (2)$$

The DBT of the model oil and the compounds produced from the desulfurization process were analyzed by GC-MS technology [65]. Before the EPODS reaction, the only detected sulfur compounds were DBT, and the products were extracted from the oil phase to the IL phase after the reaction because of the difference in polarity (Fig. 9 (d)). After the ILs phase was extracted by carbon tetrachloride and further analyzed, a large amount of $DBTO_2$ was detected. These results showed that the DBT was oxidized to the highly polar species $DBTO_2$ in the phase of ILs during the EPODS process and ultimately achieved the standard of deep desulfurization.

Based on the foregoing research, a possible mechanism of EPODS was proposed, as shown in Fig. 10. CTAC-HPW, [Hmim]Cl, H_2O_2–HCOOH, and visible light irradiation constituted the EPODS system, which had the advantages of good selectivity and excellent desulfurization activity. During the extraction process, DBT of the model oil was extracted to the IL phase and then sufficiently contacted with the photocatalyst due to the well mass transfer effect. As the system was exposed to the irradiation of visible light, since the photogenerated e^--h^+ pair separation efficiency of the photocatalyst was good (Eq. (3)), the H_2O_2 was reduced by e^- to generate ·OH and then produced ·COOH with HCOOH. With the cooperation of h^+ and ·COOH, dibenzothiophene sulfides were efficiently oxidized to the corresponding sulfone substances. Extraction and photocatalytic oxidation were carried out continuously until the ultra-low sulfur fuel was obtained. The equations of the reaction mechanism are shown below:

$$\text{CTAC-HPW} + h\nu \rightarrow e^- + h^+ \quad (3)$$

$$e^- + H_2O_2 \rightarrow \cdot OH + OH^- \quad (4)$$

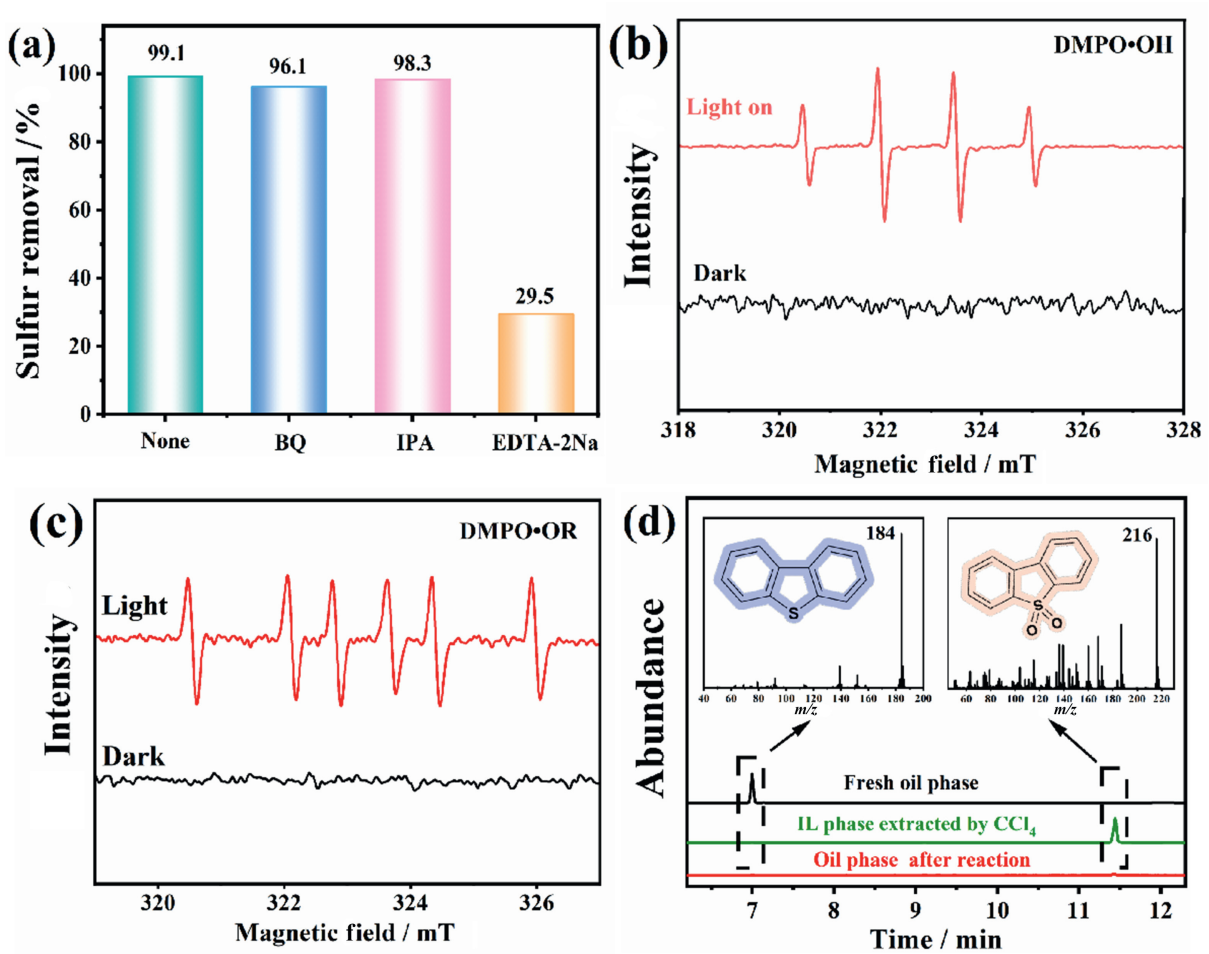

Fig. 9. The radical scavenging experiments under visible light (a). (Conditions: T = 30 °C, V (model oil) = 20 ml, m (catal.) = 0.04 g, visible light, V ([Hmim]Cl) = 1 ml, V (HCOOH) = 1 ml, V (H_2O_2) = 0.5 ml), ESR signals using CTAC-HPW of DMPO•OH (b) and DMPO•OR (c). GC-MS spectra of model oil before and after reaction (d).

$$h^+ + OH^- \rightarrow \cdot OH \quad (5)$$

$$\cdot OH + HCOOH \rightarrow \cdot COOH + H_2O \quad (6)$$

$$e^- + H_2O_2 + HCOOH \rightarrow \cdot COOH + H_2O + OH^- \quad (7)$$

$$h^+/\cdot COOH + DBT \rightarrow DBTO_2 \quad (8)$$

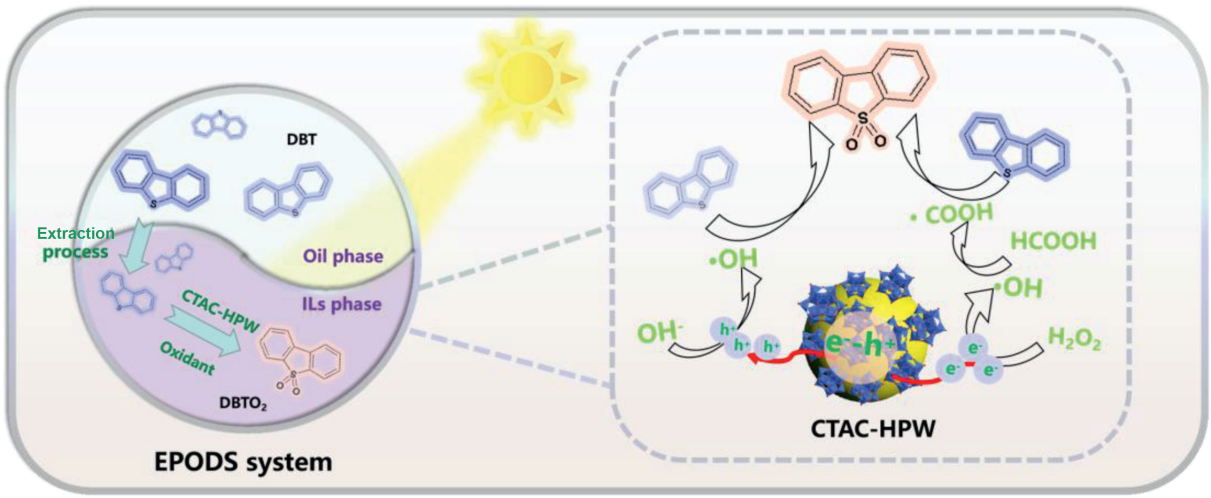

Fig. 10. The possible desulfurization reaction process.

4. Conclusions

In this research, a CTAC-HPW photocatalyst with a Keggin structure was prepared *via* the combination of the quaternary ammonium organic cation and phosphotungstate anion by electrostatic interactions and van der Waals forces. The obtained composite was used for photocatalytic desulfurization of sulfur-containing harmful substances in model oil, and the effects of different reaction conditions were studied. The photocatalyst CTAC-HPW under the conditions of H_2O_2–HCOOH as the oxidant and [Hmim]Cl as the extractant displayed prominent desulfurization performance and achieved the standard of deep desulfurization within 30 min for model oil. Moreover, CTAC-HPW possessed excellent cycling stability with low activity loss within 25 cycles. The high desulfurization performance was ascribed mainly to the coordination of extraction and photocatalytic oxidation, and h^+ and ·COOH played a main role in the oxidation process. The merits of inexpensive raw materials and facile preparation methods were conducive to efficiently converting DBT to $DBTO_2$ with added value and subservience to widen its practical application prospects in the field of desulfurization.

Declaration of Interest

The authors declare that they have no known competing financial interests or personal relationships that could have appeared to influence the work reported in this paper.

Acknowledgements

We thank the financial supports from National Natural Science Foundation of China (22172066, 22378176). This work was also supported by State Key Laboratory of Heavy Oil Processing. Supported by Jiangsu Collaborative Innovation Center of Technology and Material of Water Treatment, Suzhou University of Science and Technology.

Supplementary Material

Supplementary data to this article can be found online at https://doi.org/10.1016/j.cjche.2024.02.002.

References

[1] L. Chen, J.T. Ren, H.Y. Wang, M.L. Sun, Z.Y. Yuan, Engineering a local hydrophilic environment in fuel oil for efficient oxidative desulfurization with minimum H_2O_2 oxidant, *ACS Catal.* 13 (18) (2023) 12125–12133.
[2] G. Ye, M. Zheng, Q.L. Zhang, J. Zhou, L. Wu, J. Wang, Defect-mediated synergistic effect of POM/UiO-66(Zr) host-guest catalysts for robust deep desulfurization at ambient temperature, *Small* 19 (38) (2023) e2301035.
[3] Z. Man, Y. Meng, X.C. Lin, X.R. Dai, L.P. Wang, D.Z. Liu, Assembling UiO-66@TiO_2 nanocomposites for efficient photocatalytic degradation of dimethyl sulfide, *Chem. Eng. J.* 431 (2022) 133952.
[4] M. Ahmad, M. Yousaf, W.W. Cai, Z.P. Zhao, Formulation of heterometallic ZIF-8@Cu/Ni/ZnO@CNTs heterostructure photocatalyst for Ultra-Deep desulphurization of coal and fuels, *Chem. Eng. J.* 453 (2023) 139846.
[5] J. Zhu, J.T. Yu, P.W. Wu, J.X. Liu, H.Y. Ji, P. Cui, Y.H. Chao, W.S. Zhu, H.Y. Liu, Z.C. Liu, 3D printing of the multifunctional fixed-bed reactor and matched 3D-CeO_2/ATP monolithic adsorbent for adsorption desulfurization, *Chem. Eng. J.* 468 (2023) 143590.
[6] S. Chu, X. Li, R. Prins, C.H. Wang, Y.Y. Liu, A.J. Wang, Q. Sheng, Preparation of ultrasmall Ni2P nanoparticles with low P/Ni ratios supported on SiO_2 and an Al_2O_3-B_2O_3 mixed oxide for dibenzothiophene hydrodesulfurization, *J. Catal.* 420 (2023) 110–122.
[7] Z.H. Deng, L.S. Dai, W. Han, X.H. Cai, X.P. Nie, Q. Fang, H. Nie, Towards a deep understanding of the evolution and molecular structures of refractory sulfur compounds during deep residue hydrotreating process, *Fuel Process. Technol.* 231 (2022) 107235.
[8] Y. Muhammad, H.U. Rashid, S. Subhan, A.U. Rahman, M. Sahibzada, Z.F. Tong, Boosting the hydrodesulfurization of dibenzothiophene efficiency of Mn decorated (Co/Ni)-Mo/Al_2O_3 catalysts at mild temperature and pressure by coupling with phosphonium based ionic liquids, *Chem. Eng. J.* 375 (2019) 121957.
[9] Y. Muhammad, Y.Z. Lu, C. Shen, C.X. Li, Dibenzothiophene hydrodesulfurization over Ru promoted alumina based catalysts using *in situ* generated hydrogen, *Energy Convers. Manag.* 52 (2) (2011) 1364–1370.
[10] Y. Muhammad, C.X. Li, Dibenzothiophene hydrodesulfurization using *in situ* generated hydrogen over Pd promoted alumina-based catalysts, *Fuel Process. Technol.* 92 (3) (2011) 624–630.
[11] L.N. Zhou, Y. Du, Y.X. Jin, W.X. Chen, Q.Y. Pan, W. Kai, Y.S. Liu, L. Yang, Z.H. Liu, Grinding-induced solvent-free synthesis of mesoporous zirconia-supported tungsten oxide composite and its superior oxidative desulfurization performance, *Fuel* 315 (2022) 123181.
[12] Y.M. Ren, D.S. Feng, Z.M. Yan, Z.X. Sun, Z.X. Zhang, D.W. Xu, C. Qiao, Z.H. Chen, Y. Jia, S.C. Jun, S.D. Liu, Y. Yamauchi, Interfacial coupled engineering of plasmonic amorphous MoO_{3-x} nanodots/g-C_3N_4 nanosheets for photocatalytic water splitting and photothermal conversion, *Chem. Eng. J.* 453 (2023) 139875.
[13] J.M. Wu, X.M. Wu, P.P. Zhao, Z.H. Wang, L.Z. Zhang, D.M. Xu, J. Gao, Extraction desulphurization of fuels using ZIF-8-based porous liquid, *Fuel* 300 (2021) 121013.
[14] D. Tanikawa, S. Seo, D. Motokawa, Development of a molasses wastewater treatment system equipped with a biological desulfurization process, *Environ. Sci. Pollut. Res. Int.* 27 (20) (2020) 24738–24748.
[15] H. Liu, J. He, K. Zhu, D.A. Zhu, L.H. Zhu, W.S. Zhu, H.M. Li, W. Jiang, Modification of cobalt doped mesoporous sieve by grafting *N*, *N*-dihydroxypyromellitimide to enhance desulfurization catalyst stability, *J. Mol. Liq.* 390 (2023) 122970.
[16] Z. Moheb-Aleaba, M.R. Khosravi-Nikou, Extractive desulfurization of liquid hydrocarbon fuel using ionic liquids: Cationic and anionic selection through principal component analysis and experimental study, *J. Mol. Liq.* 384 (2023) 122211.
[17] S. Subhan, Y. Muhammad, M. Sahibzada, F. Subhan, Z.F. Tong, Studies on the selection of a catalyst–oxidant system for the energy-efficient desulfurization and denitrogenation of fuel oil at mild operating conditions, *Energy Fuels* 33 (9) (2019) 8423–8439.
[18] B.L. Li, H.Y. Song, F.Q. Han, L.S. Wei, Photocatalytic oxidative desulfurization and denitrogenation for fuels in ambient air over Ti_3C_2/g-C_3N_4 composites under visible light irradiation, *Appl. Catal. B Environ.* 269 (2020) 118845.
[19] I. Shafiq, S. Shafique, P. Akhter, G. Abbas, A. Qurashi, M. Hussain, Efficient catalyst development for deep aerobic photocatalytic oxidative desulfurization: recent advances, confines, and outlooks, *Catal. Rev.* 64 (4) (2022) 789–834.
[20] S.H. Xun, W. Jiang, T. Guo, M.Q. He, R.L. Ma, M. Zhang, W.S. Zhu, H.M. Li, Magnetic mesoporous nanospheres supported phosphomolybdate-based ionic liquid for aerobic oxidative desulfurization of fuel, *J. Colloid Interface Sci.* 534 (2019) 239–247.
[21] S.W. Li, Y.Y. Li, F. Yang, Z. Liu, R.M. Gao, J.S. Zhao, Photocatalytic oxidation desulfurization of model diesel over phthalocyanine/$La_{0.8}Ce_{0.2}NiO_3$, *J. Colloid Interface Sci.* 460 (2015) 8–17.
[22] F.M. Li, M.Q. Hua, Y.C. Wei, J.X. Liu, J.H. Gong, C. Wang, P.W. Wu, Y. Huang, H. M. Li, W.S. Zhu, Insight into the oxidative desulfurization of high-sulfur petroleum coke under mild conditions: a journey of vanadium-substituted Dawson-type phosphotungstic acid, *Petrol. Sci.* 18 (3) (2021) 983–993.
[23] Q.Q. Liu, H.Y. Lin, X.L. Wang, X. Wang, N. Xu, Y. Tian, L. Yang, X.R. Li, J.Y. Sun, Two novel polyoxometalate-based metal–organic complexes with chiral waugh-type$[MnMo_9O_{32}]^{6-}$ anions as high-efficiency catalytic oxidative desulfurization catalysts, *Cryst. Growth Des.* 21 (12) (2021) 7015–7022.
[24] R. Ghubayra, C. Nuttall, S. Hodgkiss, M. Craven, E.F. Kozhevnikova, I.V. Kozhevnikov, Oxidative desulfurization of model diesel fuel catalyzed by carbon-supported heteropoly acids, *Appl. Catal. B Environ.* 253 (2019) 309–316.
[25] U. Caudillo-Flores, F. Ansari, B. Bachiller-Baeza, G. Colón, M. Fernández-García, A. Kubacka, $(NH_4)_4[NiMo_6O_{24}H_6].5H_2O$/g-$C_3N_4$ materials for selective photooxidation of C—O and C—C bonds, *Appl. Catal. B Environ.* 278 (2020) 119299.
[26] E.I. García-López, G. Marcì, I. Krivtsov, J. Casado Espina, L.F. Liotta, A. Serrano, Local structure of supported keggin and wells–dawson heteropolyacids and its influence on the catalytic activity, *J. Phys. Chem. C* 123 (32) (2019) 19513–19527.
[27] H.M. Dong, W.H. Li, Y.Q. Ou, D. Gao, Y.B. Yang, Y.H. Zhang, P. Xiao, Self-assembly hydrothermal synthesis of silverton-type polyoxometalate-based photocatalysts for enhanced degradation, *Langmuir* 36 (16) (2020) 4454–4464.
[28] X.S. Wang, Y.B. Huang, Z.J. Lin, R. Cao, Phosphotungstic acid encapsulated in the mesocages of amine-functionalized metal-organic frameworks for catalytic oxidative desulfurization, *Dalton Trans.* 43 (31) (2014) 11950–11958.
[29] H.F. Wang, C.Y. Wang, Y.F. Yang, M. Zhao, Y.J. Wang, $H_3PW_{12}O_{40}$/mpg-C_3N_4 as an efficient and reusable bifunctional catalyst in one-pot oxidation–Knoevenagel condensation tandem reaction, *Catal. Sci. Technol.* 7 (2) (2017) 405–417.
[30] M. Craven, D. Xiao, C. Kunstmann-Olsen, E.F. Kozhevnikova, F. Blanc, A. Steiner, I.V. Kozhevnikov, Oxidative desulfurization of diesel fuel catalyzed by polyoxometalate immobilized on phosphazene-functionalized silica, *Appl. Catal. B Environ.* 231 (2018) 82–91.
[31] D. Betz, P. Altmann, M. Cokoja, W.A. Herrmann, F.E. Kühn, Recent advances in oxidation catalysis using ionic liquids as solvents, *Coord. Chem. Rev.* 255 (13–14) (2011) 1518–1540.

[32] S.H. Xun, R.M. Le, C.C. Hu, D.S. Liu, S.M. Wang, M.Q. He, W.S. Zhu, H.M. Li, Ionic liquid promotes high dispersion of V_2O_5 on 3D porous g-C_3N_4 carrier to enhance catalytic oxidative desulfurization performance, *Energy Fuels* 37 (8) (2023) 6276–6280.
[33] Y. Gao, Z. Liu, R.M. Gao, G.F. Hu, J.S. Zhao, Support ionic liquid-heteropolyacid hybrid on mesoporous carbon aerogel with a high surface area for highly efficient desulfurization under mild conditions, *Microporous Mesoporous Mater.* 305 (2020) 110392.
[34] A.A. Bryzhin, M.G. Gantman, A.K. Buryak, I.G. Tarkhanova, Brønsted acidic SILP-based catalysts with $H_3PMo_{12}O_{40}$ or $H_3PW_{12}O_{40}$ in the oxidative desulfurization of fuels, *Appl. Catal. B Environ.* 257 (2019) 117938.
[35] L.L. Wu, Z.X. Jiao, S.H. Xun, M.Q. He, L. Fan, C. Wang, W.S. Yang, W.S. Zhu, H.M. Li, Photocatalytic oxidative of Keggin-type polyoxometalate ionic liquid for enhanced extractive desulfurization in binary deep eutectic solvents, *Chin. J. Chem. Eng.* 44 (2022) 205–211.
[36] A. Akopyan, E. Eseva, P. Polikarpova, A. Kedalo, A. Vutolkina, A. Glotov, Deep oxidative desulfurization of fuels in the presence of Brönsted acidic polyoxometalate-based ionic liquids, *Molecules* 25 (3) (2020) 536.
[37] Y. Liu, J.H. Sun, H.H. Huang, L.L. Bai, X.M. Zhao, B.H. Qu, L.Q. Xiong, F.Q. Bai, J. W. Tang, L.Q. Jing, Improving CO_2 photoconversion with ionic liquid and Co single atoms, *Nat. Commun.* 14 (1) (2023) 1457.
[38] M.L. Sarazen, E. Iglesia, Stability of bound species during alkene reactions on solid acids, *Proc. Natl. Acad. Sci. U. S. A.* 114 (20) (2017) E3900–E3908.
[39] X.L. Xue, W. Zhao, B.C. Ma, Y. Ding, Efficient oxidation of sulfides catalyzed by a temperature-responsive phase transfer catalyst $[(C_{18}H_{37})_2(CH_3)_2N]_7PW_{11}O_{39}$ with hydrogen peroxide, *Catal. Commun.* 29 (2012) 73–76.
[40] S.J. Zhang, G.D. Zhao, S. Gao, Z.W. Xi, J. Xu, Secondary alcohols oxidation with hydrogen peroxide catalyzed by$[n\text{-}C_{16}H_{33}N(CH_3)_3]_3PW_{12}O_{40}$: Transform-and-retransform process between catalytic precursor and catalytic activity species, *J. Mol. Catal. Chem.* 289 (1–2) (2008) 22–27.
[41] A.S. Krishna Kumar, S.J. Jiang, W.L. Tseng, Effective adsorption of chromium(vi)/Cr(iii) from aqueous solution using ionic liquid functionalized multiwalled carbon nanotubes as a super sorbent, *J. Mater. Chem. A* 3 (13) (2015) 7044–7057.
[42] X.Y. Jiang, Z.Y. Zhang, M.H. Sun, W.Z. Liu, J.D. Huang, H.Y. Xu, Self-assembly of highly-dispersed phosphotungstic acid clusters onto graphitic carbon nitride nanosheets as fascinating molecular-scale Z-scheme heterojunctions for photocatalytic solar-to-fuels conversion, *Appl. Catal. B Environ.* 281 (2021) 119473.
[43] X.Y. Zeng, X.Y. Xiao, J.Y. Chen, H.L. Wang, Electron-hole interactions in choline-phosphotungstic acid boosting molecular oxygen activation for fuel desulfurization, *Appl. Catal. B Environ.* 248 (2019) 573–586.
[44] S. Subhan, M. Yaseen, B. Ahmad, Z.F. Tong, F. Subhan, W. Ahmad, M. Sahibzada, Fabrication of MnO_2 NPs incorporated UiO-66 for the green and efficient oxidative desulfurization and denitrogenation of fuel oils, *J. Environ. Chem. Eng.* 9 (3) (2021) 105179.
[45] M. Yaseen, S. Subhan, F. Subhan, A.U. Rahman, A. Naeem, Z. Ahmad, Z. Tong, Hausmannite Mn_3O_4 functionalized graphene Oxide-NaClO system for oxidative desulfurization and denitrogenation of fuel oils, *Fuel* 321 (2022) 124017.
[46] S. Subhan, A. Ur Rahman, M. Yaseen, H. Ur Rashid, M. Ishaq, M. Sahibzada, Z. F. Tong, Ultra-fast and highly efficient catalytic oxidative desulfurization of dibenzothiophene at ambient temperature over low Mn loaded Co-Mo/Al_2O_3 and Ni-Mo/Al_2O_3 catalysts using NaClO as oxidant, *Fuel* 237 (2019) 793–805.
[47] M. Yaseen, S. Ullah, W. Ahmad, S. Subhan, F. Subhan, Fabrication of Zn and Mn loaded activated carbon derived from corn cobs for the adsorptive desulfurization of model and real fuel oils, *Fuel* 284 (2021) 119102.
[48] Ashfaq, S. Subhan, A. Ur Rahman, B. Ahmad, K. Khan, F. Subhan, W. Ahmad, M. Yaseen, Nickel impregnated graphene oxide catalyst for thedesulfurization of transportation fuels using NaClO/H_2O_2 oxidants, *Petrol. Sci. Technol.* (2023) 1–21.
[49] C.C. Hu, S.H. Xun, D.S. Liu, L.H. Zhu, M.Q. He, Q.H. Zhang, H.M. Li, W.S. Zhu, Construction of 3D mesoporous silica supported MoO_3 nanoparticles for the efficient photocatalytic oxidative desulfurization under visible light, *Sep. Purif. Technol.* 334 (2024) 126032.
[50] L.Y. Zhang, Q. Hou, Y. Zhou, J. Wang, Phosphotungstic anion-paired quinoline salt for heterogeneous photocatalytic hydroxylation of benzene to phenol with air, *Mol. Catal.* 473 (2019) 52–61.
[51] H. Luo, Y.Q. Huang, H.L. Liu, B. Zhang, J. Song, Ionic liquid assisted pure blue emission $CsPbBr_3$ quantum dots with improved optical properties and alkyl chain regulated stability, *Chem. Eng. J.* 430 (2022) 132790.
[52] H.M. Salem, D. Mohmed, E.G. Zaki, Nanoarchitectonics of copper tungsten-mesoporous silica with a new template for photo oxidative-desulfurization of dibenzothiophene, *J. Inorg. Organomet. Polym. Mater.* 32 (10) (2022) 3725–3737.
[53] S. Mohammadzadeh Yengejeh, S. Allahyari, N. Rahemi, Efficient oxidative desulfurization of model fuel by visible-light-driven MoS_2-CeO_2/SiO_2-Al_2O_3 nano photocatalyst coating, *Process. Saf. Environ. Prot.* 143 (2020) 25–35.
[54] A.S. Morshedy, H.R. Ali, A.A. Nada, A.M. Rabie, H.H. El-Maghrabi, Highly efficient imprinted polymer nanocomposites for photocatalytic desulfurization of real diesel fuel, *Environ. Technol. Innov.* 21 (2021) 101206.
[55] G. Dashtpeyma, S.R. Shabanian, Efficient photocatalytic oxidative desulfurization of liquid petroleum fuels under visible-light irradiation using a novel ternary heterogeneous $BiVO_4$-CuO/modified natural clinoptilolite zeolite, *J. Photochem. Photobiol. Chem.* 445 (2023) 115024.
[56] L. Wang, Z. Ning, M. Sun, Y.Y. Ma, N. Mominou, W.J. Jiang, S.Z. Li, C.Y. Jing, Deep desulfurization and denitrogenation of diesel fuel over Ir/Pr-N-CQDs-TiO_2 under ultraviolet radiation, *Sep. Purif. Technol.* 272 (2021) 118861.
[57] H.Z. Chang, H. Yi, J.W. Zhang, Preparation of a NiO-Bi_2WO_6 catalyst and its photocatalytic oxidative desulfurization performance, *Colloid Interface Sci. Commun.* 41 (2021) 100381.
[58] O. Amiri, F. Beshkar, S.S. Ahmed, P.H. Mahmood, A.A. Dezaye, Hierarchical *p*-BiOI/*n*-$BiPO_4$ heterojunction nanocomposite with enhanced visible-light photocatalytic desulfurization of thiophene under mild conditions, *Int. J. Hydrogen Energy* 46 (9) (2021) 6547–6560.
[59] M. Siahmansouri, M. Mousavi-Kamazani, Photocatalytic desulfurization of thiophene under visible light by hollow flower-like NiZnVO/WO nanostructures, *Ceram. Int.* 47 (19) (2021) 27241–27250.
[60] S.H. Xun, C.C. Wu, L.D. Tang, M.M. Yuan, H.F. Chen, M.Q. He, W.S. Zhu, H.M. Li, One-pot *in situ* synthesis of coralloid supported VO_2 catalyst for intensified aerobic oxidative desulfurization, *Chin. J. Chem. Eng.* 56 (2023) 136–140.
[61] H.P. Li, W.S. Zhu, S.W. Zhu, J.X. Xia, Y.H. Chang, W. Jiang, M. Zhang, Y.W. Zhou, H.M. Li, The selectivity for sulfur removal from oils: An insight from conceptual density functional theory, *AIChE J.* 62 (6) (2016) 2087–2100.
[62] Z.H. Wang, W.H. Ma, C.C. Chen, H.W. Ji, J.C. Zhao, Probing paramagnetic species in titania-based heterogeneous photocatalysis by electron spin resonance (ESR) spectroscopy—A mini review, *Chem. Eng. J.* 170 (2–3) (2011) 353–362.
[63] X.Y. Zeng, X.Y. Xiao, Y. Li, J.Y. Chen, H.L. Wang, Deep desulfurization of liquid fuels with molecular oxygen through graphene photocatalytic oxidation, *Appl. Catal. B Environ.* 209 (2017) 98–109.
[64] J.J. Yang, D.X. Li, Q.L. Li, Z.J. Zhang, H.Q. Wang, Mechanism of photocatalytic oxidation of formaldehyde, *Acta Phys. Chim. Sin.* 17 (2001) 278–281.
[65] M. Yaseen, M. Ullah, S. Subhan, W. Ahmad, F. Subhan, M. Shakir, Recovery and characterization of useful benzene derivatives from spent engine oil through solvent extraction, *Chem. Eng. Res. Des.* 175 (2021) 51–60.